Accepted Manuscript

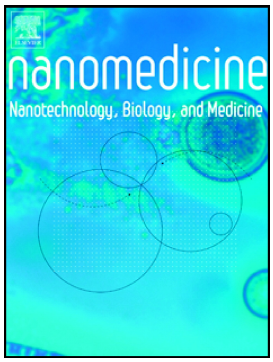

Smart nanoparticles assembled by endogenous molecules for siRNA delivery and Cancer therapy via CD44 and EGFR dual-targeting

Yaoyao Liang, Jiahui Peng, Ning Li, Cynthia Yu-Wai-Man, Qian Wang, Yuhong Xu, Hongxia Wang, Aristides D Tagalakis, Zixiu Du

PII: S1549-9634(18)30537-9
DOI: doi:10.1016/j.nano.2018.09.018
Reference: NANO 1884

To appear in: *Nanomedicine: Nanotechnology, Biology, and Medicine*

Revised date: 5 September 2018

Please cite this article as: Yaoyao Liang, Jiahui Peng, Ning Li, Cynthia Yu-Wai-Man, Qian Wang, Yuhong Xu, Hongxia Wang, Aristides D Tagalakis, Zixiu Du , Smart nanoparticles assembled by endogenous molecules for siRNA delivery and Cancer therapy via CD44 and EGFR dual-targeting. Nano (2018), doi:10.1016/j.nano.2018.09.018

Smart Nanoparticles Assembled by Endogenous Molecules for siRNA Delivery and Cancer Therapy via CD44 and EGFR Dual-targeting

Yaoyao Liang[a], Jiahui Peng[a], Ning Li[b], Cynthia Yu-Wai-Man[c], Qian Wang[a], Yuhong Xu[a], Hongxia Wang[*, b], Aristides D Tagalakis[d], Zixiu Du[*, a]

[a]School of Pharmacy, Shanghai Jiao Tong University, 800 Dongchuan Road, Shanghai 200240, P.R. China

[b]Department of Oncology, Shanghai General Hospital, Shanghai Jiao Tong University School of Medicine, 227 South Chongqing Road, Shanghai 201620, P.R. China

[c]National Institute for Health Research (NIHR) Biomedical Research Centre at Moorfields Eye Hospital NHS Foundation Trust and UCL Institute of Ophthalmology, 162 City Road, London EC1V 2PD, UK

[d]Department of Biology, Edge Hill University, Ormskirk, L39 4QP, UK

*Correspondences: Hongxia Wang, Tel: +8621 37798551, E-mail: whx365@126.com. Zixiu Du, Tel. +82 34204739, Fax +82 34204457, E-mail: zixiudu@sjtu.edu.cn.

Word count for Abstract: 150

Word count for manuscript: 4157 (including Abstract, Introduction, Methods, results, Discussion and Figure legends)

Number of References: 39

Number of figures: 7

Number of tables: 0

Number of Supplementary online-only files: 1

Statement

The authors declare no competing financial interests. This work was supported by the National Natural Science Foundation of China (No. 81690262) and the Engineering and Medical Cooperation Projects of Shanghai Jiao Tong University (No. YG2016MS22) and Minhang "Production-Study-Research" Project in Sanghai (No. 2016MH229). The development fund for Shanghai talents (No. 2017111)

Abstract

We developed an anticancer siRNA delivery system (named HLPR) through modular assembly of endogenous molecules. The structure of HLPR was a tightly condensed siRNA-peptide inner core in turn surrounded by the disordered lipid layer and thin HA coating from which the EGFR-targeted amino acid sequences of IVNQPTYGYWHY partially protrude outside of cell surfaces. Both HA and IVNQPTYGYWHY anchored on HLPR were responsible for targeting CD44 and EGFR overexpressed on the tumor cell surfaces, respectively. HLPR was relatively stable in the blood circulation and reached at the tumor tissue in vivo through passive and active targeting. Then HLPR entered tumor cells mainly through EGFR-mediated pathway followed by the separation of HA from the remaining parts of nanocomplexes. The HA-uncoated complexes escaped the endosome through the membrane fusion function of DOPE and released cargoes (siRNA and peptide/siRNA) in the cytoplasm. HLPR significantly inhibited the growth of implanted subcutaneous liver tumors without toxicity.

Keywords: dual targeting, CD44 and EGFR, multifunctional peptide, tumor, HA coating

Introduction

Chemical drug treatment of tumor has been utilized for cancer therapy but is associated with non-specific cytotoxicity.(1) On the contrary, RNA interference (RNAi) mediated through small interfering RNA (siRNA) has been proved to be a highly efficient and promising therapeutic platform for malignant and genetic diseases due to its ability of target-specific gene silencing at post-transcriptional level.(2) Survivin is prominently expressed during embryonal development and absent in most normal.(3) Survivin expression in cancer tissues is associated with not only apoptosis inhibition but also resistance to conventional treatment and malignancy of tumors. These features make it a unique and important target for cancer therapy.(4) Survivin siRNA has been considered as an important biological drug to silence the survivin gene at the mRNA level for tumor treatment. SiRNAs are prone to degradation by the nucleases in the extracellular environment and in addition, as anionic macromolecules, they are less capable to interact with the negative surface of tumor cells.(5) Thus, an in vivo suitable delivery vehicle has to be developed for siRNA targeting transportation in cancer treatment.

To date, poor delivery efficiency in vivo is the major hurdle hampering expectations in ultimately transforming siRNA into clinical practice. Compared with the viral siRNA delivery system, the non-viral vectors have the advantages of unlimited packaging capacity and no integration into the genome.(6) To successfully deliver siRNA to the tumor area and avoid nonspecific binding, degradation and elimination in the biological fluid, development of efficacious delivery systems, such as nano-vectors, have been applied to improve efficacy and overcome several physiological barriers of siRNA trafficking.(7) The ideal nano-vectors should be utilized for “stealth” circulation outside of tumor tissues and then successfully pass through the leaky endothelium and

actively enter into the cancer cells and release the cargoes into the cytoplasm.(5) To achieve this aim, the nanoparticles should not only have suitable sizes and enough stability for circulating and passing through the tumor vessels but also have the abilities for harboring various target moieties to actively bind receptors that are overexpressed at the membrane of tumor cells.(8) Furthermore, the siRNA vectors should also be able to tackle the intracellular barriers and release their cargoes in the cytoplasm.(7)

Nanoparticles for siRNA targeted delivery have long been studied as a particularly promising drug delivery vehicle.(9) Many of the targeted delivery systems, assembled by cationic polymers and amphiphilic compounds, have been used to directly introduce siRNA into the cancer cells.(10-12) For example, Liu et al. reported the multifunctional polymer/siRNA polyplexes for tumor-targeted siRNA delivery,(13) Kostarelos et al. constructed the ABCD lipoplexes.(14) In addition, the lipopolyplexes assembled by liposome/protamine/siRNA(15) and receptor-targeted nanocomplexes (RTNs) designed through modular strategy(16) and inorganic nanocomplexes modified by biomaterials(17) have been reported as anticancer delivery systems. Despite these advances, there is no clinical product of non-viral vectors that target other organs beyond the liver due to either high-chemical toxicity of vectors or being not very stable in the extracellular blood circulation(18). Protecting the structure of the nano-delivery system until reaching the tumor cells is crucial for in vivo targeted delivery. In addition, the biocompatibility of vectors and the antitumor effectiveness of the nanoparticles must be fully considered during the design process of the delivery system.

CD44 overexpressed at the membrane surface of tumor cells is distinct from those of the normal tissues, and hyaluronic acid (HA) can

specifically target CD44 proteins overexpressed at the membrane surface of cancer cells but not targeting those of the normal cells(19). Thus, HA was utilized as the targeting moiety for anticancer targeting delivery(20). Epidermal growth factor receptor (EGFR), as one of the overexpressed transmembrane proteins in most cancer cells, is also a specific receptor for the targeted delivery system for anticancer drugs. GE11 (YHWYGYTPQNVI), as an EGFR-targeted peptide selected through phage display technology,(21) was positioned on the surface of anticancer drug vectors to achieve specific delivery. (22)

To completely overcome the in vivo physiological barriers and achieve targeted delivery without safety and low-delivery efficiency issues, we have recently constructed an optimized siRNA delivery system via specific penetrating hepatic tumor cells termed Q-complexes.(23, 24) In the present study, we used GE11 replacing the penetrating amine acid sequences (KRPTMRFRYTWNPMK)(25) and kept unaltered the other compositions to construct a tumor dual-targeted drug delivery system (termed HLPR). We hypothesized that HLPR has similar structure with Q-complexes but possess dual-targeting moieties to strengthen the specific delivery. HLPR also has good stability in the blood circulation to deliver siRNA to tumors and silence the target gene. This work is exploring the design of a dual-targeting tumor siRNA delivery system by using Food and Drug Administration (FDA)-approved biomaterials through modular strategy. The aim was to develop a suitable siRNA targeted delivery system that could be utilized for anticancer clinical application.

Methods

Animals

All animal experiments animals were approved by the Laboratory Animal Centre of Shanghai Jiao Tong University and were performed according to the guideline of the

National Institutes of Health for the humane care and use of laboratory animals (NIH publication No. 8023).

In vivo imaging

The major tissues (heart, liver, spleen, lung, and kidney) and tumor were dissected, collected, and imaged using the IVIS Lumina II small-animal imaging system (Caliper Life Sciences, Alameda, CA, USA). A Cy5 filter set was used to acquire Cy5-siRNA fluorescence values in vivo. Images were acquired and analyzed using the Living Image 4.3.1 software (Caliper Life Sciences, Alameda, CA, USA).

In vivo biochemical and efficacy assay

Mice bearing transplanted HCCLM3 hepatic carcinoma were established as described in Supplementary materials. The in vivo function markers of liver and kidney and blood glucose were measured on Beckman Coulter AU5800 (Beckman Coulter, CA, USA) in Shanghai General Hospital. After euthanization, the body and tumor weights of mice were measured. For histological studies, the tumors were sectioned at 4 μm and examined with hematoxylin–eosin (H&E)(26) (Beyotime, Shanghai, China. In addition, the TdT-mediated dUTP nick-end labeling (TUNEL) staining (Bosterbio, CA, USA) and immunohistochemistry (IHC) staining (Abcam, Cambridge, UK) for survivin protein were performed according to the manufacturers' protocols.(27) The histological sections were observed under an optical microscope (DP72, Olympus).

Statistical analysis

Data are presented as mean ± standard deviation and compared using Student's t-tests. Statistically significant differences were expressed as "ns" represents $p > 0.05$, "*" represents $p < 0.05$, "**" represents $p < 0.01$, "***" represents $p < 0.001$. Analyses were performed using GraphPad Instat software (GraphPad, San Diego, CA, USA).

Results

Formulation and characterization of HLPR

A schematic diagram of the assembly of HLPR nanocomplexes is shown in Figure 1A. First, LPR was formed by the assembly of DOTAP/DOPE liposome, multifunctional peptide (GE11R16), and siRNA at the weight ratios of 1:4:1 in aqueous solution. The size of LPR was 81.4 ± 3.2 nm and the zeta potential of LPR nanoparticles was +59 ± 0.9 mV (Figure 1B). When the weight ratio of HA to siRNA was 14:1, the size and zeta potential of nanocomplexes did not change with further increases of HA to siRNA ratios (data not shown). This finding indicated that the above weight ratio of HA to siRNA completely shielded the cationic internal core, and this optimized formulation was selected for all subsequent studies. Compared with LPR, the zeta potential of HLPR rapidly reversed to −36 ± 0.6 mV, and the size of HLPR slightly increased to 108 ± 4.07 nm (Figure 1C). The morphologies of LPR and HLPR were observed with Transmission Electron Microscopy (TEM). Sphere shapes with a diameter of approximately 50 nm, which is smaller than the size examined by DLS, was found in all of them. To mimic the interference of albumin in vivo with the nanocomplexes, LPR and HLPR were incubated for 24 h in 5% bovine serum. The results showed that the size of HLPR kept constant within the timeframe tested, whereas the size of LPR rapidly increased to 3500 nm and then decreased to the original diameters, when the charge of LPR reversed from positive to negative. The zeta potential of HLPR was slightly increased but remained negative in the same conditions (Figure 1D). At the same time, the HLPR size was unchangeable in 10% FBS and RPMI-1640 (Table S1) within 12 h. Gel electrophoresis assay was used to examine the release of siRNA in the serum. The result showed that siRNA packaged in LPR was released within 4 h at 37 °C in 67% FBS, whereas siRNA packaged in HLPR was only released after being incubated for 9 h at the same condition (Figure 1E). This finding indicated that HLPR has

relatively high stability to protect siRNA in the serum for more than twice the time compared to LPR. The observed stability of HLPR is likely attributed to LPR being tightly shielded by HA.

Mechanism of cell uptake

HCCLM3 cells were selected to explore the siRNA delivery of HLPR. Both Cy5-labeled siRNA and fluorescein isothiocyanate labeled HA (FITC-HA) were utilized to examine the cell uptake efficiency of HLPR. Chlorpromazine and anti-CD44-antibody were used to inhibit the EGFR and CD44-mediated pathways, respectively. We found that both HA and siRNA entered the cells through the CD44-independent and EGFR-dependent pathways (Figures 2A and B). The internalization of HLPR was also investigated through confocal laser scanning microscopy (CLSM). FITC-HA and Cy5-siRNA were utilized to track the signal paths of HA and siRNA. We found that most FITC-HA and Cy5-siRNA were located together but not completely colocalizing at 45 min (Figure 2C), indicating that some of FITC-HA have begun to dissociate from Cy5-siRNA at this time point. However, we only observed FITC signal and not that of Cy5-siRNA at 4 h (Figure 2D). This phenomenon demonstrated that HA had completely separated from the other components of HLPR, indirectly supporting the result of the flow cytometry assay that showed HLPR was first endocytosed, then, HA component was separated from the other components of HLPR.

siRNA delivery efficiency and cytotoxicity of HLPR

Lipofectamine 2000 (L_2K), as an efficient transfection reagent, was used as the positive control to investigate the transfection efficiency at cell level. The cytotoxicity studies (Figure 3A), revealed that the viability of HCCLM3 cells transfected with HLPR or LPR was higher than that of L_2K. qPCR and apoptosis assays (that stained the nucleus with Hoechst 33342) also showed that HLPR has the capability to deliver siRNA to the cell cytoplasm and

exert its effects there (Figures 3B and C). HLPR containing survivin siRNA silenced approximately 90% of the gene at the mRNA level compared with that of HLPR containing negative siRNA.

In vivo tissue distribution of siRNA and the influence of HLPR on the normal tissues

The in vivo heart, liver, spleen, lung, kidney, and tumor distributions of siRNA delivered by HLPR were examined through tracking the fluorescence of Cy5-labeled siRNA. Most fluorescence 6 h after administration was observed in the kidney and tumor of mice in the HLPR group as shown in Figure 4A. Moreover, the fluorescence of naked Cy5-siRNA was only found in the kidney, and little fluorescence could be observed in the tumor. No Cy5-siRNA was found in the heart and spleen. At the same time, very little fluorescence was observed in the liver and lung. The fluorescence of tumors in the HLPR group was nearly three times higher than that in mice of the siRNA group ($p<0.05$; Figure 4B). To further examine the toxicity of HLPR and the influence of HLPR on normal tissues, the concentrations of blood glucose and those of the conventional functional indicators of the liver and kidney were tested from the peripheral blood following eight administrations of siRNA or controls every other day at a dose of 1 mg/kg siRNA. As shown in Figure 5, the HLPR-survivin group and the untreated group had equivalent levels at most of the examined indicators. It indicated that HLPR was nontoxic in vivo and showed no negative effect on the normal tissues and the concentration of blood glucose.

In vivo antitumor efficacy

The antitumor efficacy of HLPR-survivin siRNA was investigated in mice bearing HCCLM3 tumors. From the result of tumor volume changes of each group (Figure 6A), it was shown that the tumors in siRNA and HLPR-negative groups grew rapidly over time and had no obvious difference compared with the tumor growth of the untreated group. However, the tumor

growth of the HLPR-survivin group was significantly inhibited and reached only one fourth of the average volume compared with the glucose control group. As shown in Figure 6B, the mouse weights of all groups were not affected during repeat administrations, indicating that the vectors have no toxicity in vivo. The final tumor weights (Figure 6C) and the tumor images of each group (Figure 6D) also demonstrated that the tumors of the HLPR-survivin group were significantly smaller compared with the other groups.

Then, the tumors from the in vivo studies were investigated for cell proliferation and apoptosis using H&E and TUNEL staining (Figures 7A and B). Nuclei of hematoxylin-labeled cells were stained blue and the eosin-labeled cytoplasms were stained red in H&E. Nuclei of proliferating cell nuclear antigen (PCNA)-labeled cells were stained brown by ABC method in TUNEL. Tumors from HLPR-survivin-injected mice exhibited a markedly higher count of purple and brown-colored PCNA-labeled cells compared with the control or other groups as shown in Figures 7A and 7B, respectively. This finding showed more advanced and more extensive apoptosis and necrosis of tumors in the HLPR-survivin group than the other treatments. To further elucidate the mechanisms of the suppression of survivin gene, the HCCLM3 tumors of mice were also investigated using the IHC assay. As shown in Figure 7C, survivin proteins of IHC-positive cells were stained brown and the nuclei were stained blue. The images indicated that the number of brown spots dramatically decreased in the HLPR-survivin group compared with those in the other groups, indicating that the HLPR formulation containing survivin siRNA silenced its target gene at the protein level.

Discussion

HLPR was designed through a modular strategy, characterized by the assembly of each component through noncovalent bonding to form various

functional nanocomplexes.(23) Without the chemical covalence between the components, the chemical safety and biocompatibility of modular formulation were predictable and controllable. We focused on EGFR and CD44 overexpressed on the tumor cell surface as the targeted receptors for specific delivery of cancer drugs. (28) GE11, an EGFR-targeted peptide was used to design a novel multifunctional peptide (GE11R16, IVNQPTYGYWHYRRRRRRRRRRR RRRR) for formulating HLPR as the similar designed-strategy reported in our previous study.[23, 24] HLPR were negatively charged nanocomplexes, the physicochemical characteristics of which were stable compared with the highly positive charge of LPR in the serum. This phenomenon indicated that HA coated on LPR completely shielded the positive surface charge and greatly delayed the release time of siRNA in the serum (Figure 1E). It showed that HLPR is more capable to protect its cargoes than LPR in the circulation in vivo.

As reported by Mustapa et al. (29), the lipid-peptide-nucleic acid structure of LPR should comprise of a tightly condensed nucleic acid-peptide inner core surrounded by a disordered lipid layer, wherein the integrin-targeting sequence of the peptide should also partially protrude due to the electrically neutral amine acid sequences of GE11 (Figure 1A). The structure of LPR has the smart capability for tightly wrapping siRNA and actively binding the targeted cells compared with cationic liposome/siRNA (LR) and peptide/siRNA nanocomplexes (PR); thus, LPR showed significantly enhanced transfection efficiency in vitro compared with LR and PR (16). However, as a positively charged nanocomplex, LPR has the limitation that in vivo its targeting capability is reduced due to nonspecific binding to the negative surface of normal tissues and cells. Other caveats of cationic nanoparticles include interaction with serum components and rapid clearance from the circulation. Anionic nanocomplexes are now being

investigated further by different groups as an approach to circumvent the problems associated with the in vivo use of cationic nanoparticles. Anionic formulations have been used for siRNA silencing with promising results, including tumor targeting. (30-33) Therefore, there is a need to optimize the design, formulation and potential applications of anionic nanocomplexes. Thus, the additional assembly of LPR and HA at the optimized ratio was investigated for in vivo circulation and specific delivery to tumor through enhanced permeability and retention (EPR) effect and active target of CD44 and EGFR overexpressed on the surface of cancer cells. The highly negative charge and much better stability of HLPR compared to LPR in the serum, indicated that HA could tightly coat on the surface of the disordered lipid layer of DOTAP/DOPE mainly through electrostatic interaction. Moreover, some of the other noncovalent bonding, such as hydrogen bond between HA and the exposure acid amine sequences of the multifunctional peptide component (23), further stabilized the adherence of HA component on the surface of LPR. Given that GE11 assisted in cellular internalization mainly via the clathrin-mediated endocytosis pathway (34), we studied the cell uptake mechanism of HLPR in the presence of anti-CD44-antibody and chlorpromazine (an inhibitor of clathrin-dependent endocytosis) (35) to investigate the targeting function of HA and GE11. The results indicated that both HA and siRNA components of HLPR entered HCCLM3 cells through CD44-independent and clathrin-dependent pathways. The findings here show that HA and siRNA components of HLPR did not dissociate from each other before being endocytosed. This study indirectly proved that the structure of HLPR was similar with that of LPR and GE11 sequences of multifunctional peptide component partially protruding outside of HLPR (Figure 1A).

In vitro, HLPR had comparable siRNA delivery efficiency with LPR and

L_2K This finding showed that HA not only shielded the positive charge of LPR but also improved the affinity of negatively charged nanocomplexes to tumor cells through the dual-targeting by HA and GE11 sequences of CD44 and EGFR, respectively, that are overexpressed on the surface of HCCLM3 cells. This factor is a special advantage of HA to actively bind to the cancer cells compared with the other anionic polymers. Interestingly, we found that HA began to dissociate from the nanocomplexes after HLPR was endocytosed by HCCLM3 cells (Figures 3C and D). The in vivo siRNA delivery results also indicated that HLPR were stable enough to circulate in the blood. There was fluorescence detected in other organs (mainly in the kidneys and some in the lung and liver) but this could be attributed to the time point of imaging. Later time points (e.g. 24 hours) would potentially show more accumulation in the tumor and far less in first-pass organs such as the kidneys.(36) Overall the tissue distributions of Cy5-siRNA fluorescence in vivo, show that HLPR formulation firstly utilized the electronegativity of HA resulting in extended circulation lifetimes and then demonstrated the ability to specifically target CD44 for enhanced adhesion to the tumor. As shown in Figure 1A on the model of HLPR construction, the HA component looked similar to an "outerwear with many little bores" on the surface of LPR nanocomplexes, and the GE11 sequences partially protrude from the bores. Then, the anchored GE11 sequences on the surface of HLPR strongly bound the EGFR that is overexpressed on the cancer cell surface, and HLPR was endocytosed through an EGFR-mediated pathway, which is a smart process of HLPR to overcome the extracellular biological barriers. During endocytosis, the HA component of HLPR probably started to dissociate from LPR. Next, DOPE disrupted the endosomal membrane(37) to release siRNA and peptide/siRNA complexes into the cytoplasm. The proposed pathway of the HLPR smart vector is shown in Figure S3. We found that HLPR was a suitable tumor-targeting

delivery system for anticancer treatment in the tumors that overexpress at the cell surface CD44 and EGFR proteins. The liver and kidney biochemical assays and the weight of mice that was unaffected by the repeat administration regime, demonstrated that the HLPR vectors were nontoxic in vivo. The great inhibition of tumor growth in the HLPR-survivin group compared with that of the other groups and, in addition, the extensive apoptosis and necrosis of tumors, indicated that HLPR was a highly efficient siRNA delivery system and has the potential for clinically pharmaceutical applications. As tumor progression is complex to study and target with a single target gene, in the future we will investigate whether combination therapy (e.g. multiple siRNAs) can not only inhibit tumor growth but also reduce tumor volume.

From the above investigation, we found that HLPR is a novel attractive self-assembled system compared with the universal lipopolyplexes (38) and PEGylated RTNs reported previously (39). Lipopolyplexes always consist of a polyplex core and a liposomal shell, which had to conjugate in turn with PEG and targeting ligands to achieve targeted delivery. For PEGylated RTNs, the PEG chains and integrin-targeting peptides protrude from the same disordered lipid layer. The PEG chains would weaken the targeting function of integrin-targeting peptides, and the optimized percentage of PEG and targeting moieties are always difficult to control accurately. Thus, the pharmaceutical preparation of PEGylated RTNs is challenging to produce, indicating that PEGylation of RTNs would either reduce the delivery capability of siRNA vectors or incompletely shield the positive charge. HLPR formulation overcomes the disadvantages of universal lipopolyplexes and RTNs. A postulated mechanism for the efficient transfection of HLPR nanocomplexes is described. This study supports a novel and rational strategy for effective siRNA delivery in vivo.

References

1. Kinoshita R, Ishima Y, Chuang VTG, Nakamura H, Fang J, Watanabe H, et al. Improved anticancer effects of albumin-bound paclitaxel nanoparticle via augmentation of EPR effect and albumin-protein interactions using S-nitrosated human serum albumin dimer. Biomaterials. 2017;140:162-9.

2. Hannon GJ. RNA interference. Nature. 2002;418(6894):244-51.

3. Lopergolo A, Tavecchio M, Lisanti S, Ghosh JC, Dohi T, Faversani A, et al. Chk2 phosphorylation of survivin-DeltaEx3 contributes to a DNA damage-sensing checkpoint in cancer. Cancer research. 2012;72(13):3251-9.

4. Yang FF, Huang W, Li YF, Liu S, Jin MJ, Wang YL, et al. Anti-tumor effects in mice induced by survivin-targeted siRNA delivered through polysaccharide nanoparticles. Biomaterials. 2013;34(22):5689-99.

5. Yin H, Kanasty RL, Eltoukhy AA, Vegas AJ, Dorkin JR, Anderson DG. Non-viral vectors for gene-based therapy. Nature reviews Genetics. 2014;15(8):541-55.

6. Riley MK, Vermerris W. Recent Advances in Nanomaterials for Gene Delivery-A Review. Nanomaterials. 2017;7(5).

7. Xin Y, Huang M, Guo WW, Huang Q, Zhang LZ, Jiang G. Nano-based delivery of RNAi in cancer therapy. Molecular cancer. 2017;16(1):134.

8. Dobiasch S, Szanyi S, Kjaev A, Werner J, Strauss A, Weis C, et al. Synthesis and functionalization of protease-activated nanoparticles with tissue plasminogen activator peptides as targeting moiety and diagnostic tool for pancreatic cancer. Journal of nanobiotechnology. 2016;14(1):81.

9. Ferrari M. Frontiers in cancer nanomedicine: directing mass transport through biological barriers. Trends in biotechnology. 2010;28(4):181-8.

10. Tatiparti K, Sau S, Kashaw SK, Iyer AK. siRNA Delivery Strategies: A Comprehensive Review of Recent Developments. Nanomaterials. 2017;7(4).

11. Roberts CM, Shahin SA, Wen W, Finlay JB, Dong J, Wang R, et al. Nanoparticle delivery of siRNA against

TWIST to reduce drug resistance and tumor growth in ovarian cancer models. Nanomedicine : nanotechnology, biology, and medicine. 2017;13(3):965-76.

12. Xu H, Li Z, Si J. Nanocarriers in gene therapy: a review. Journal of biomedical nanotechnology. 2014;10(12):3483-507.

13. Liu L, Zheng M, Librizzi D, Renette T, Merkel OM, Kissel T. Efficient and Tumor Targeted siRNA Delivery by Polyethylenimine-graft-polycaprolactone-block-poly(ethylene glycol)-folate (PEI-PCL-PEG-Fol). Molecular pharmaceutics. 2016;13(1):134-43.

14. Kostarelos K, Miller AD. Synthetic, self-assembly ABCD nanoparticles; a structural paradigm for viable synthetic non-viral vectors. Chemical Society reviews. 2005;34(11):970-94.

15. Chono S, Li SD, Conwell CC, Huang L. An efficient and low immunostimulatory nanoparticle formulation for systemic siRNA delivery to the tumor. Journal of Controlled Release. 2008;131(1):64-9.

16. Tagalakis AD, He L, Saraiva L, Gustafsson KT, Hart SL. Receptor-targeted liposome-peptide nanocomplexes for siRNA delivery. Biomaterials. 2011;32(26):6302-15.

17. Jin WH, Wang QW, Wu M, Li Y, Tang GP, Ping Y, et al. Lanthanide-integrated supramolecular polymeric nanoassembly with multiple regulation characteristics for multidrug-resistant cancer therapy. Biomaterials. 2017;129:83-97.

18. Riley MK, Vermerris W. Recent Advances in Nanomaterials for Gene Delivery-A Review. Nanomaterials-Basel. 2017;7(5).

19. Bachar G, Cohen K, Hod R, Feinmesser R, Mizrachi A, Shpitzer T, et al. Hyaluronan-grafted particle clusters loaded with Mitomycin C as selective nanovectors for primary head and neck cancers. Biomaterials. 2011;32(21):4840-8.

20. Hwang DW, Kim HY, Li F, Park JY, Kim D, Park JH, et al. In vivo visualization of endogenous miR-21 using hyaluronic acid-coated graphene

oxide for targeted cancer therapy. Biomaterials. 2017;121:144-54.

21. Li Z, Zhao R, Wu X, Sun Y, Yao M, Li J, et al. Identification and characterization of a novel peptide ligand of epidermal growth factor receptor for targeted delivery of therapeutics. FASEB journal : official publication of the Federation of American Societies for Experimental Biology. 2005;19(14):1978-85.

22. Mondal G, Kumar V, Shukla SK, Singh PK, Mahato RI. EGFR-Targeted Polymeric Mixed Micelles Carrying Gemcitabine for Treating Pancreatic Cancer. Biomacromolecules. 2016;17(1):301-13.

23. Xie F, Zhang L, Peng J, Li C, Pu J, Xu Y, et al. Hepatic Carcinoma Selective Nucleic Acid Nanovector Assembled by Endogenous Molecules Based on Modular Strategy. Molecular pharmaceutics. 2017;14(6):1841-51.

24. Zhang L, Li Z, Sun F, Xu Y, Du Z. Effect of inserted spacer in hepatic cell-penetrating multifunctional peptide component on the DNA intracellular delivery of quaternary complexes based on modular design. International journal of nanomedicine. 2016;11:6283-95.

25. Kondo E, Saito K, Tashiro Y, Kamide K, Uno S, Furuya T, et al. Tumour lineage-homing cell-penetrating peptides as anticancer molecular delivery systems. Nature communications. 2012;3:951.

26. Wang Y, Shi KR, Zhang L, Hu GL, Wan JY, Tang JJ, et al. Significantly enhanced tumor cellular and lysosomal hydroxychloroquine delivery by smart liposomes for optimal autophagy inhibition and improved antitumor efficiency with liposomal doxorubicin. Autophagy. 2016;12(6):949-62.

27. Kim IY, Kang YS, Lee DS, Park HJ, Choi EK, Oh YK, et al. Antitumor activity of EGFR targeted pH-sensitive immunoliposomes encapsulating gemcitabine in A549 xenograft nude mice. Journal of Controlled Release. 2009;140(1):55-60.

28. Liang X, Shi B, Wang K, Fan M, Jiao D, Ao J, et al. Development of self-assembling peptide nanovesicle with bilayers for enhanced

EGFR-targeted drug and gene delivery. Biomaterials. 2016;82:194-207.

29. Mustapa MFM, Bell PC, Hurley CA, Nicol A, Guenin E, Bell PC, et al. Biophysical characterization of an integrin-targeted lipopolyplex gene delivery vector. Biochemistry-Us. 2007;46(45):12930-44.

30. Kapoor M, Burgess DJ. Cellular uptake mechanisms of novel anionic siRNA lipoplexes. Pharmaceutical research. 2013;30(4):1161-75.

31. Tagalakis AD, Lee DH, Bienemann AS, Zhou H, Munye MM, Saraiva L, et al. Multifunctional, self-assembling anionic peptide-lipid nanocomplexes for targeted siRNA delivery. Biomaterials. 2014;35(29):8406-15.

32. Yang XZ, Du JZ, Dou S, Mao CQ, Long HY, Wang J. Sheddable ternary nanoparticles for tumor acidity-targeted siRNA delivery. ACS nano. 2012;6(1):771-81.

33. Tagalakis AD, Castellaro S, Zhou H, Bienemann A, Munye MM, McCarthy D, et al. A method for concentrating lipid peptide DNA and siRNA nanocomplexes that retains their structure and transfection efficiency. Int J Nanomedicine. 2015;10:2673-83.

34. Zhang MZ, Li C, Fang BY, Yao MH, Ren QQ, Zhang L, et al. High transfection efficiency of quantum dot-antisense oligonucleotide nanoparticles in cancer cells through dual-receptor synergistic targeting. Nanotechnology. 2014;25(25):255102.

35. Marina-Garcia N, Franchi L, Kim YG, Hu YJ, Smith DE, Boons GJ, et al. Clathrin- and Dynamin-Dependent Endocytic Pathway Regulates Muramyl Dipeptide Internalization and NOD2 Activation. J Immunol. 2009;182(7):4321-7.

36. Tagalakis AD, Maeshima R, Yu-Wai-Man C, Meng J, Syed F, Wu LP, et al. Peptide and nucleic acid-directed self-assembly of cationic nanovehicles through giant unilamellar vesicle modification: Targetable nanocomplexes for in vivo nucleic acid delivery. Acta Biomater. 2017;51:351-62.

37. Du Z, Munye MM, Tagalakis AD, Manunta MD, Hart SL. The role of the helper lipid on the DNA transfection

efficiency of lipopolyplex formulations. Scientific reports. 2014;4:7107.

38. Li SD, Huang L. Nanoparticles evading the reticuloendothelial system: Role of the supported bilayer. Bba-Biomembranes. 2009;1788(10):2259-66.

39. Tagalakis AD, Grosse SM, Meng QH, Mustapa MFM, Kwok A, Salehi SE, et al. Integrin-targeted nanocomplexes for tumour specific delivery and therapy by systemic administration. Biomaterials. 2011;32(5):1370-6.

Figure legends

Figure 1 Formulation and physiochemical characterization of LPR and HLPR. **(A)** Schematic diagram of the model construction of LPR and HLPR. **(B)** Distribution of diameter (b_1), zeta potential (b_2), and the morphology observed from TEM of LPR (b_3). **(C)** Distribution of diameter (c_1), zeta potential (c_2), and the morphology observed from TEM of HLPR (c_3). **(D)** Particle size and zeta potential with time of LPR and HLPR in 5% (w/v) bovine serum albumin. **(E)** Stability assay of LPR and HLPR in the serum at 0, 2, 4, 6, 7.5, 9, and 12 h. 1 represents fetal bovine serum, 2 represents naked siRNA, 3 represents LPR, 4 represents HLPR, and 5 represents the marker.

Figure 2 (A) Cellular uptake of Cy5-siRNA of LPR and HLPR and **(B)** cell uptake of FITC-HA of HLPR in HCCLM3 cells incubated for 4 h in the absence of any inhibitor (Normal) and in the presence of anti-CD44-antibody or chlorpromazine (an inhibitor of clathrin-dependent endocytosis). **(C)** and **(D)** Confocal microscopic images of the intracellular localization of HLPR identified by FITC-HA (green) and Cy5-siRNA (red) after being incubated with HCCLM3 cells for 45 min and 4 h, respectively. The nucleus is identified using DAPI (blue). Panels C1–D1 indicate DAPI-labeled nucleus (blue). Panels C2–D2 show FITC-HA (green). Panels C3–D3 identify the localization of Cy5-siRNA (red). C4–D4 represent the merged images showing the localization of FITC-HA (green) and Cy5-siRNA (red) and nucleus (blue). Scale bar = 12.5 μm for all images.

Figure 3 (A) Cytotoxicity of nanocomplexes in HCCLM3 cells 4 h after transfection. **(B)** Relative expression of survivin gene at the mRNA level in HCCLM3 cells compared with that of negative control siRNA packaged by Lipofectamine 2000, LPR,

and HLPR incubated for 48 h. **(C)** Apoptosis assay in HCCLM3 cells staining nucleus with hochest33342.

Figure 4 (A) Tissue distribution of Cy5-siRNA in the heart, liver, spleen, lung, kidneys, and tumor 6 h after an intravenous injection of physiological saline (Untreated), naked Cy5-siRNA (siRNA), and HLPR complexes containing Cy5-siRNA (HLPR), respectively. Color scale: min = 1.5×10^8, max = 4×10^9. **(B)** Mean fluorescence intensity of Cy5-siRNA in the different groups at the 6 h time point.

Figure 5 In vivo liver and kidney functional markers and the concentration of blood glucose examined in the peripheral blood of mice.

Figure 6 In vivo antitumor efficacy of siRNA administrations. **(A)** The tumor growth, **(B)** the weight changes of mice, **(C)** the tumor weights, and **(D)** the tumor images of each group of mice (n=5) after eight administrations (every other day).

Figure 7 Histological assessments of tumors following eight administrations every other day. **(A)** Hematoxylin–eosin (H&E), **(B)** TdT-mediated dUTP nick-end labeling (TUNEL), and **(C)** immunohistochemistry staining assay. A1–C1 represent the untreated group. A2–C2 represent the naked siRNA group. A3–C3 represent the HLPR-negative control siRNA (HLPR-negative) group. A4–C4 represent the HLPR-survivin group.

Figure 1

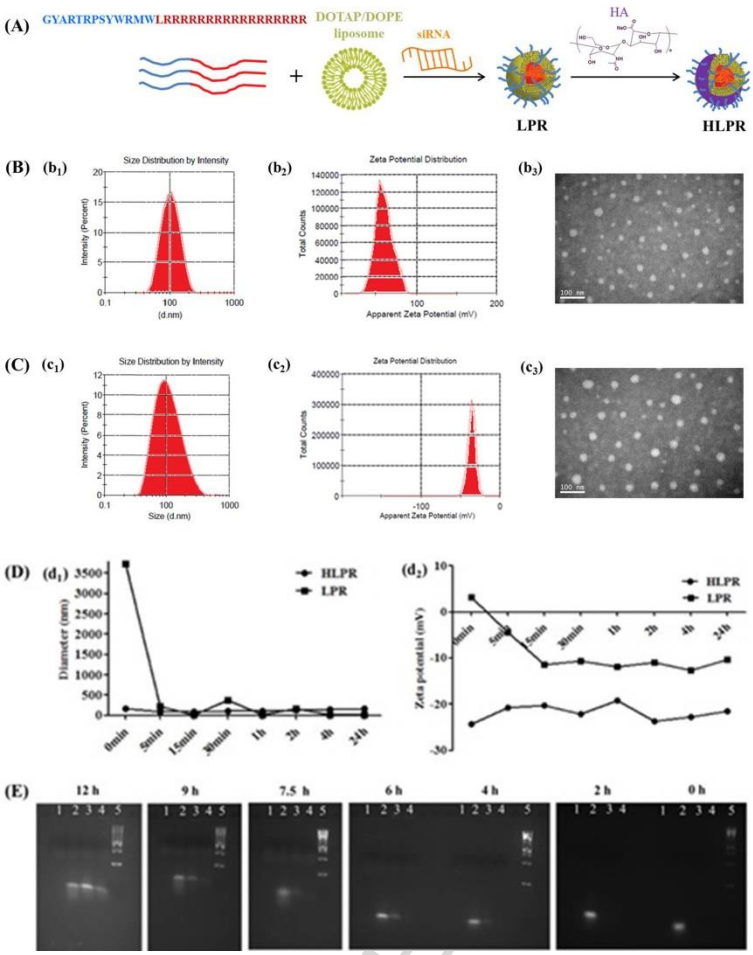

Figure 2

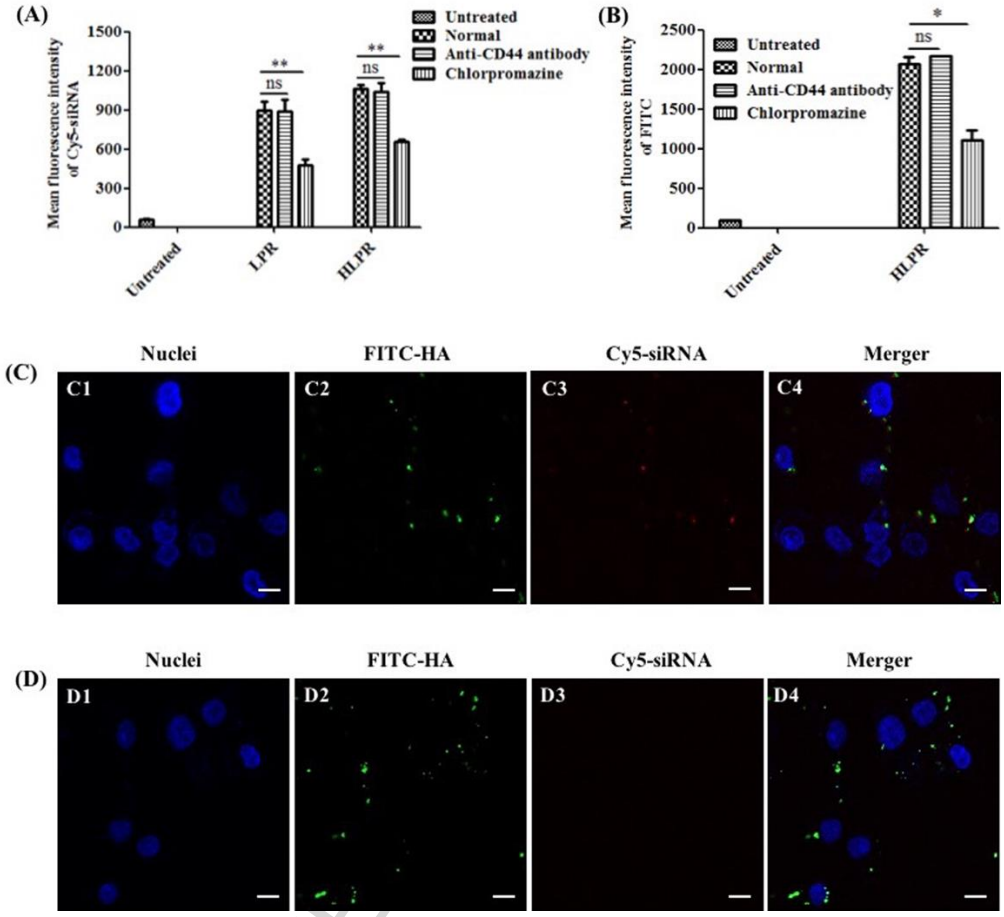

Figure 3

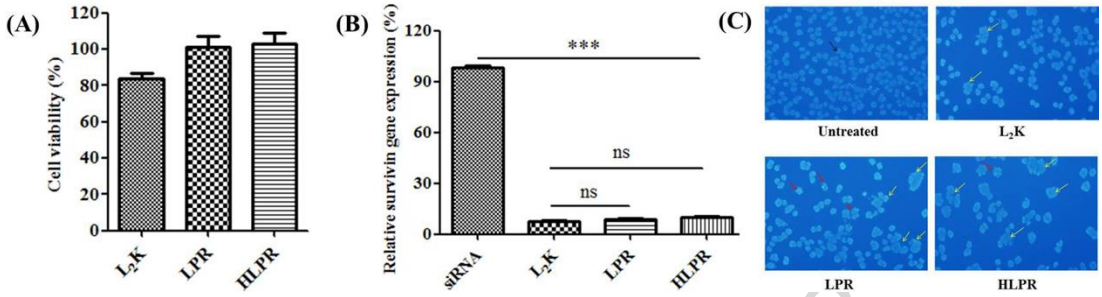

Figure 4

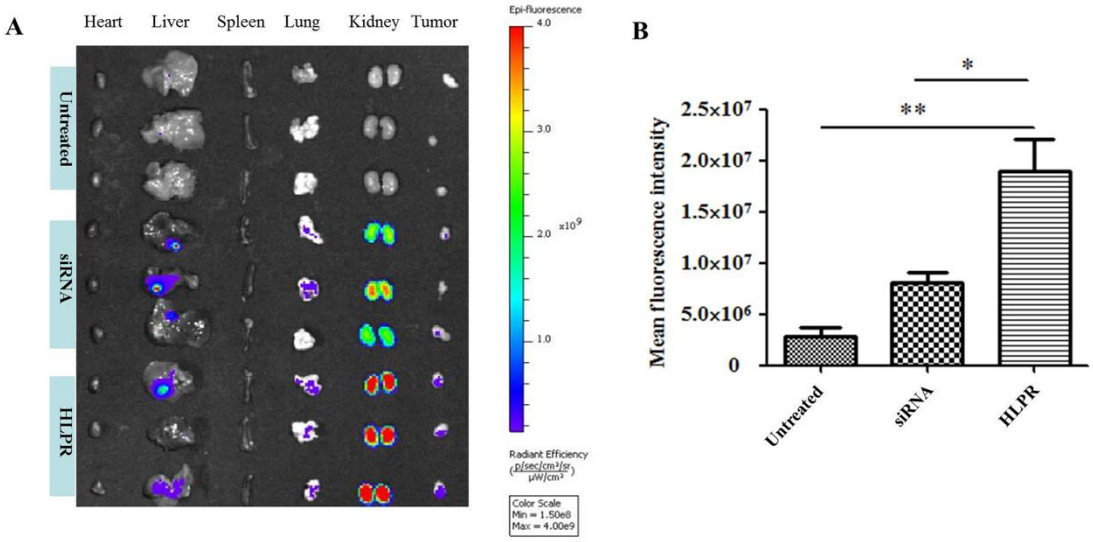

Figure 5

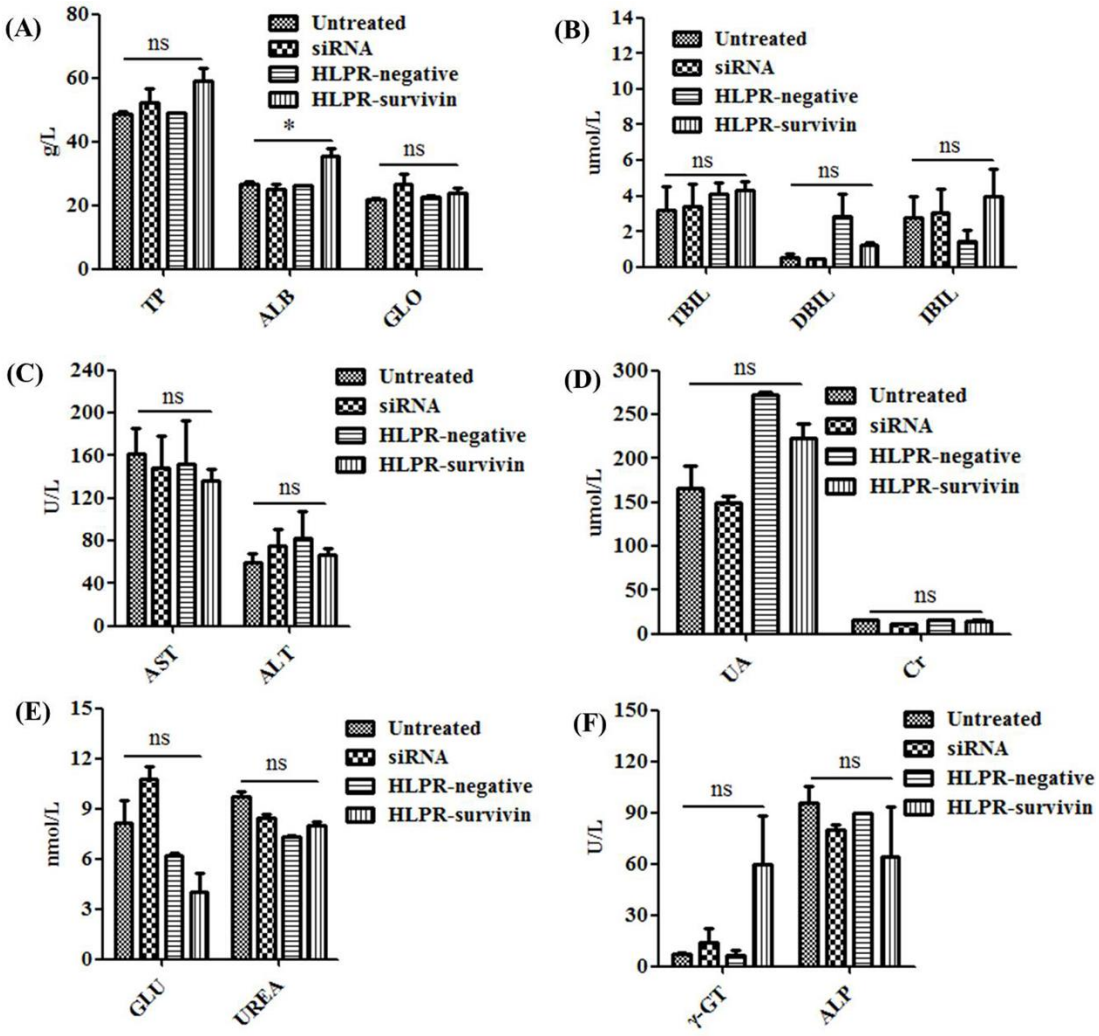

Figure 6

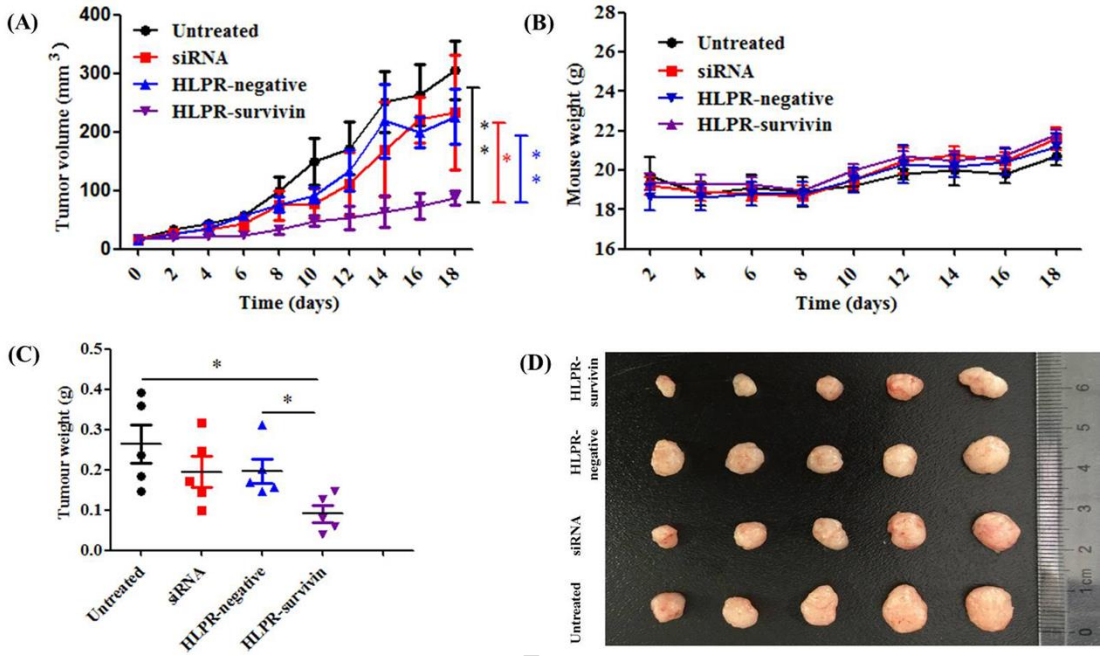

Figure 7

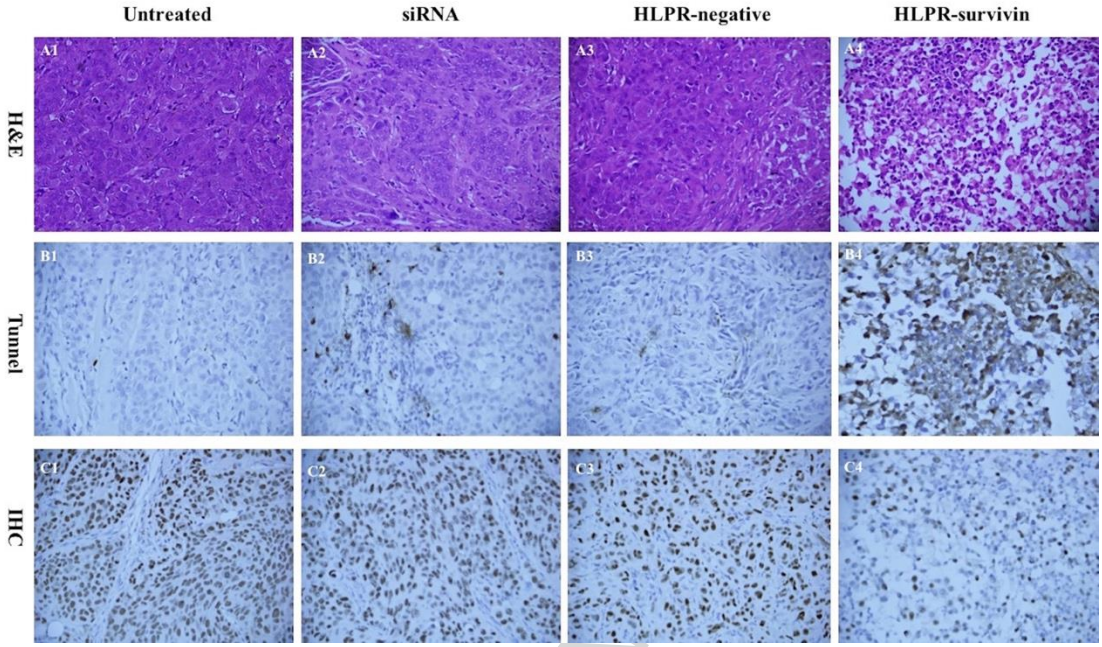

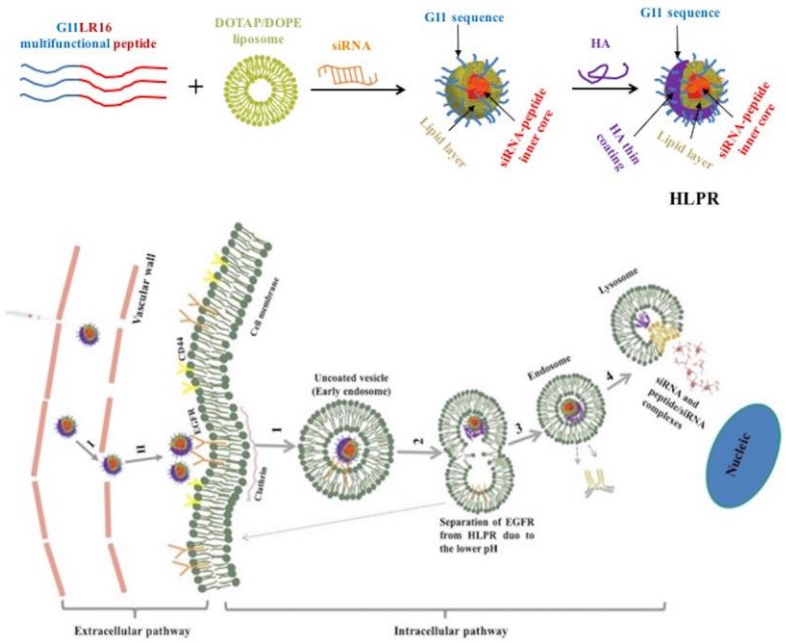

Graphical Abstract